Smart Structures and Systems, *Vol. 26, No. 5* (*2020*) *657-666*
DOI: https://doi.org/10.12989/sss.2020.26.5.657

Development of rotational pulse-echo ultrasonic propagation imaging system capable of inspecting cylindrical specimens

Hasan Ahmed[a], Young-Jun Lee[b] and Jung-Ryul Lee[*]

Department of Aerospace Engineering, Korean Advanced Institute for Science and Technology, 291 Daehak-ro, Yuseong-gu, Daejeon 305-701, Republic of Korea

(*Received March 20, 2020, Revised July 1, 2020, Accepted August 7, 2020*)

Abstract. A rotational pulse-echo ultrasonic propagation imager that can inspect cylindrical specimens for material nondestructive evaluations is proposed herein. In this system, a laser-generated ultrasonic bulk wave is used for inspection, which enables a clear visualization of subsurface defects with a precise reproduction of the damage shape and size. The ultrasonic waves are generated by a Q-switched laser that impinges on the outer surface of the specimen walls. The generated waves travel through the walls and their echo is detected by a Laser Doppler Vibrometer (LDV) at the same point. To obtain the optimal Signal-to-Noise Ratio (SNR) of the measured signal, the LDV requires the sensed surface to be at a right angle to the laser beam and at a predefined constant standoff distance from the laser head. For flat specimens, these constraints can be easily satisfied by performing a raster scan using a dual-axis linear stage. However, this arrangement cannot be used for cylindrical specimens owing to their curved nature. To inspect the cylindrical specimens, a circular scan technology is newly proposed for pulse-echo laser ultrasound. A rotational stage is coupled with a single-axis linear stage to inspect the desired area of the specimen. This system arrangement ensures that the standoff distance and beam incidence angle are maintained while the cylindrical specimen is being inspected. This enables the inspection of a curved specimen while maintaining the optimal SNR. The measurement result is displayed in parallel with the on-going inspection. The inspection data used in scanning are mapped from rotational coordinates to linear coordinates for visualization and post-processing of results. A graphical user interface software is implemented in C++ using a QT framework and controls all the individual blocks of the system and implements the necessary image processing, scan calculations, data acquisition, signal processing and result visualization.

Keywords: nondestructive material evaluation; laser ultrasonic; bulk wave propagation; rotational scan; cylinder inspection

1. Introduction

Nondestructive Evaluation (NDE) is a vast field that has received significant attention in recent years. Various NDE methods have been developed hitherto, ranging from simple visual inspection to more advanced methods using microwave, x-ray and ultrasonic waves (Panwar and Lee 2018, Schrapp *et al*. 2013). Ultrasonic Testing (UT) offers an effective evaluation of subsurface defects for both conventional and composite materials without the risk of radiation exposure. Conventional UT is based on a contact probe used in conjunction with a couplant that maximizes the energy transfer from a probe to a specimen surface (Schmerr Jr 2016). Over the years this technique has been employed for inspection of various structures including curved rotators of circular shape (Zhang *et al*. 2018). However it requires the submersion of specimen in a water tank which may affect the performance of certain materials due to humidity absorption. Some noncontact UT methods using air-coupled transducers have also been proposed; however, these methods require the probe to be in close proximity to the evaluated specimen (Hillger *et al*. 2014). Recently, laser-based UT has gained significant attention owing its ability to generate broadband ultrasounds of diverse modes in media in a noncontact manner (Scruby and Drain 1990). Laser-based UT is a noncontact method that does not require a couplant, thereby enabling the probe to operate at a distance from the specimen (Sohn and Krishnaswamy 2004, White 1963).

The evolution of laser UT in recent years has resulted in several different system arrangements, each with its own advantages. These systems can be broadly classified into guided wave and bulk wave systems, based on the nature of the ultrasonic waves used for the inspection. Systems based on in-plane guided waves (Abbas and Shafiee 2018, Petcher and Dixon 2017) require an analysis of multimode Lamb waves by complex post-processing algorithms (Flynn *et al*. 2013). This has been utilized by researchers for evaluation of circular shapes like pipes (Lee and Park 2015, Lee *et al*. 2011) but the exact evaluation of the shape and size of damages is difficult owing to the dispersive nature of Lamb waves (Rose 2014). By contrast, systems utilizing through-the-thickness bulk waves are better suited for the evaluation of thickness-related damages owing to the nondispersive

*Corresponding author, Professor,
E-mail: leejrr@kaist.ac.kr
[a] Ph.D., E-mail: ahmedhasan@kaist.ac.kr
[b] Ph.D., E-mail: 20jun@kaist.ac.kr

ISSN: 1738-1584 (Print), 1738-1991 (Online)

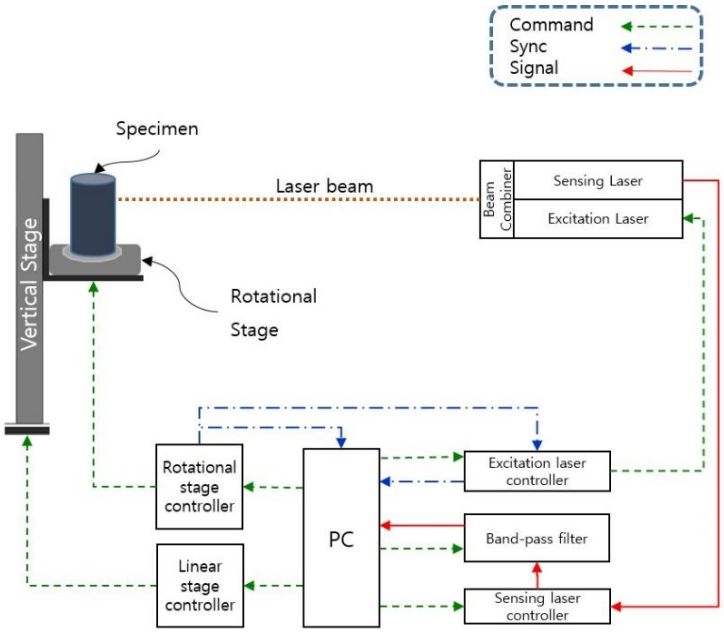

Fig. 1 R-PE UPI system setup and block diagram

nature of these longitudinal waves in their short travel times. This yields superior visualization and evaluation of defects with simple post-processing algorithms (Lee *et al*. 2018). To fully utilize laser UT, both the generation and sensing of ultrasonic signals should be laser based. Pulse-echo ultrasonic propagation imaging utilizes excitation and a sensing laser to generate and detect through-the-thickness ultrasounds in specimens. The system functions by combining the beams of excitation and sensing lasers such that the specimen is impinged by two beams simultaneously at the same spot. A Q-switched pulsed laser is used as an excitation laser and a Laser Doppler Vibrometer (LDV) as a sensing laser. The specimen under test can then be inspected by scanning its surface with the combined beam. This scanning can be performed either by using multiaxis mechanical manipulators (Zhang *et al*. 2019) or by optically steering the laser beam through a laser mirror scanner (Abbas and Lee 2018).

However, regardless of the scanning technique, using LDVs for sensing poses two constraints in terms of the position and orientation of the specimen. First, the distance between the LDV laser head and the sensed surface should be set to the pre-advised constant value for the lens used in the LDV. Next, the laser beam should be aligned to the normal of the surface when impinging on the measurement point. Both conditions must be satisfied to achieve an optimal Signal-to-Noise Ratio (SNR) of the measured signal. Because an inspection comprises multiple measurement points, both constraints should be satisfied throughout the scan. Owing to these constraints, an optical steering system (Abbas and Lee 2018) that yields faster inspection times is limited in terms of its scan area size when inspecting the planar specimen. Whereas a dual-axis linear stage system such as that in (Hong *et al*. 2016) does not have any limitations regarding the scan area size other than the physical limits of the platform. However, it is only suitable for the inspection of flat specimens as it cannot adjust the angle or distance of the laser head owing to the limited freedom of movement. Nonetheless, demand for the NDE of cylinders composed of either alloys or composites is strong.

This paper details the development and operation of a Rotational scan Pulse-Echo Ultrasonic Propagation Imager (R-PE_UPI) that enables the scan of cylindrical specimens while satisfying the constraints posed by the sensing LDV. In this system, a rotational stage is coupled with a single-axis linear stage to enable the inspection of the desired area on the specimen. This system arrangement ensures that the standoff distance and beam angle are maintained at optimal values, while the cylindrical specimen is being inspected. Moreover, the rotational scan in the system, as opposed to the raster scan (Hong *et al*. 2016), enables a continuous scanning of the inspection area without any stoppages, thereby ensuring the minimum possible inspection time for the given speed of the rotational stage and the scan resolution. The rotational scan measurements are mapped to linear coordinates for result visualization and further post-processing.

The remainder of this paper is organized into four sections. Section 2 explains the developed system and its operations. Important aspects of system operation, such as synchronization and measurement organization, are detailed in this section. Section 3 includes results that demonstrate the system operation and its ability in displaying subsurface defects. Finally, concluding remarks are provided in Section 4.

2. Rotational pulse-echo ultrasonic propagation imager

2.1 System overview

The R-PE_UPI system comprises an excitation and a

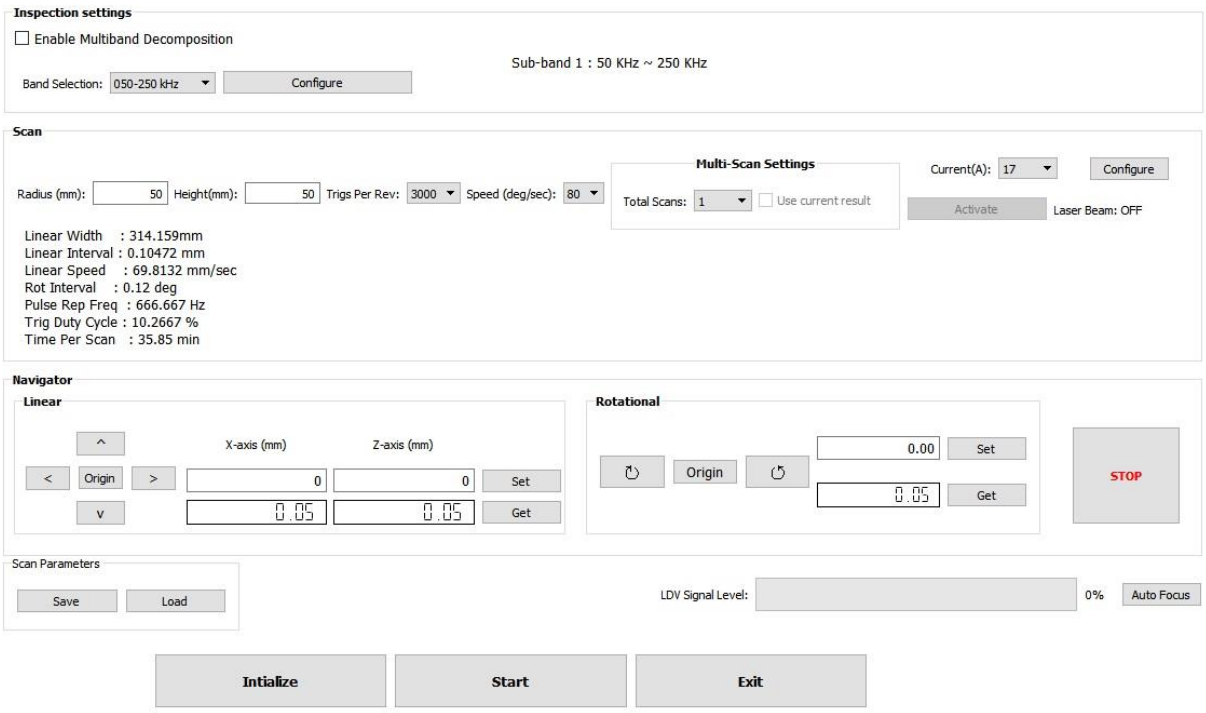

Fig. 2 Experimental setting tabs in graphical user interface

sensing laser to generate and detect through-the-thickness ultrasounds in a noncontact manner. The system is configured in a pulse-echo arrangement, whereby both the generation and sensing of ultrasound are performed at the same side of the specimen. Fig. 1 illustrates the different blocks of the system and their connections. To generate the ultrasounds, a 1053 nm solid-state Q-switched laser was used, and ultrasonic signal sensing was performed by a continuous wave LDV. The LDV employs a helium neon laser of 633 nm wavelength. A combined laser head comprising both the laser heads along with an optical mirror arrangement for beam merging was used.

The specimen to be inspected was mounted on a rotational stage, which was then mounted on a vertical stage to enable the scanning of the desired specimen height. The laser head was placed in front of the specimen such that the combined laser beam could impinge on its surface. The distance between the laser head and the specimen was adjusted to produce an optimal SNR for the signal measured by the LDV. The angle of incidence of the laser beam was adjusted such that the beam was always normal to the point of impact on the surface of the cylinder. The Graphical User Interface (GUI) software executing in a standard PC configures all the blocks of the system. The setting tab of the software interface is shown in Fig. 2. The power of the excitation laser was configured according to the characteristics of the specimen such that a sufficiently strong ultrasound could be generated without ablation. The filtering range for the measured signal was selected according to the characteristics and specifications of the specimen. The stages were controlled from the PC through their respective controllers, and the navigator in the GUI enabled the user to move the specimen for setting the start position of the inspection.

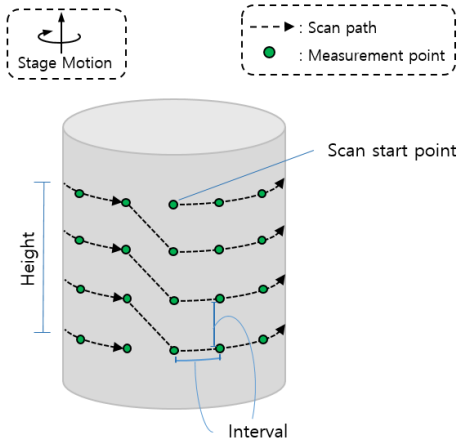

Fig. 3 Scan path and measurement pattern

2.2 Scan mechanism

The R-PE_UPI system uses the rotational and vertical stages simultaneously to scan the specimen and creates a grid of equidistant ultrasonic measurements encompassing the inspected area. Fig. 3 shows the overall scan path and the measurements. Multiple rotational scan lines over the height of the inspected area constituted a full scan, and the movement of each stage was in the opposite direction of the scan path. The scan parameters, such as resolution, height, and speed were selected a priori by the user, and each stage controller was programmed based on these selected parameters. The rotational stage controller generated 5 V transistor–transistor level trigger signals based on the distance encompassed by the stage. The Trigger-Per-Revolution (TPR) parameter, as the name suggests,

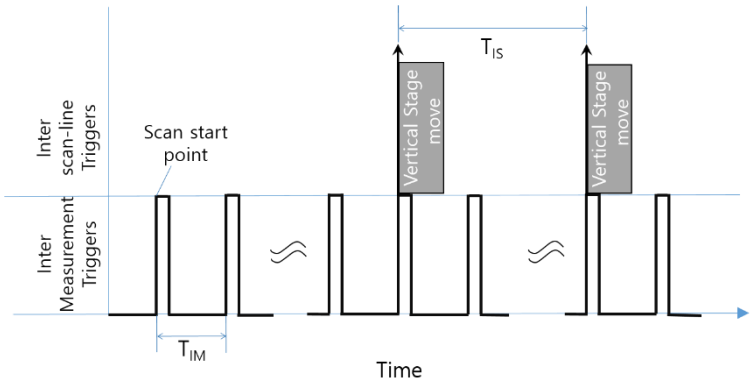

Fig. 4 Inter scan-line and inter measurement triggers

specifies the number of triggers to be generated in a single revolution. The rotational stage controller, in a single revolution of scan, generates a number of trigger signals according to the TPR.

Each rising edge of the trigger signal causes the excitation laser to emit a pulse and subsequently the Data Acquisition (DAQ) card to record the measurement via the LDV. Therefore, the TPR defines the inter-measurement interval in a rotational scan line. The completion of a revolution and hence a scan line is signaled by the rotational stage controller via an Interrupt Service Routine (ISR). This ISR functions as an inter-scan-line trigger and moves the vertical stage equal by the scan interval to start the next scan line.

Fig. 4 shows the timing and relation of these inter-measurement and inter-scan-line triggers. The rotational interval (I_R) and the inter-measurement trigger time (T_{IM}) were determined by the TPR. The vertical axis interval is the linear interval (I_L) of the scan that is calculated from the rotational interval (I_R); hence, the scan resolution is the same in both the rotational and vertical directions. The inter-scan-line time (T_{IS}) is the time consumed by the rotational stage to complete a revolution. The following equations show these relations based on the association between linear and rotational motion (Connolly 2016)

$$I_R = \frac{360}{TPR} \tag{1}$$

$$T_{IM} = \frac{I_R}{\omega} \tag{2}$$

$$I_L = \frac{2\pi . R . I_R}{360} \tag{3}$$

$$T_{IS} = \frac{360}{\omega} \tag{4}$$

where all the times are in s, the rotational speed (ω) is in °/s, and the specimen radius (R) is in mm. Because each scan-line is mapped to linear coordinates for result analysis, I_L can be regarded as the interval of the inspection. Further details regarding the result composition are included in the next section. The inspection speed can be controlled by selecting the rotational speed (ω) of the scan before the start of the inspection. Higher rotational speeds, as permitted by the weight of the specimen, are preferred for reducing the inspection time. The rotational stage supports a maximum revolution speed of 80°/s with a resolution of 0.001° and a maximum centered payload of 180 kg.

To ensure optimal scan times, no slowdown or stoppage of revolutions were ensured during the scan-line transition. In this continuous scan method, to ensure inter-scan-line alignments, the speed (v) for the vertical stage movement was calculated based on the current values of ω and I_L. The vertical stage speed was set sufficiently high to ensure the recording of the first measurement point of the subsequent scan-line at the correct position. Therefore, the measurement points of all the rotational scan lines were perfectly aligned and any side effects, such as vibrations owing to sudden vertical movements, were minimized.

2.3 Measurement organization

During the scan, at each measurement point, the 16-bit DAQ digitized the ultrasonic wave sensed by the LDV. These measurements were transferred to the PC in real time via direct memory access. A first-in first-out buffer was maintained in the on-board memory of the DAQ to avoid any overwrites on the measurements that were not yet transferred to the PC. The measurements received in the PC were stored in the physical memory for fast access and processing. A three-dimensional data structure of size ($C \times H \times T$) was maintained for storing these measurements, where C denotes the circumference of the inspected specimen, H the scan height, and T the length of each measurement in the samples. As each measurement was digitized at a sampling rate of 10 MHz for a duration of 51.2 µs, the value of T was fixed at 512 samples.

The arrangement of measurements in the buffer can be expressed in the array form as follows

$$M(t) = \begin{bmatrix} m(t)_{1,1} & \cdots & m(t)_{x,1} \\ \vdots & \ddots & \vdots \\ m(t)_{1,y} & \cdots & m(t)_{x,y} \end{bmatrix} \quad \text{where } x \le \frac{C}{I_L}, \quad y \le \frac{H}{I_L} \tag{5}$$

where $m(t)_{x,y}$ is the digitized signal from the x^{th} measurement point of the y^{th} rotational scan line of the

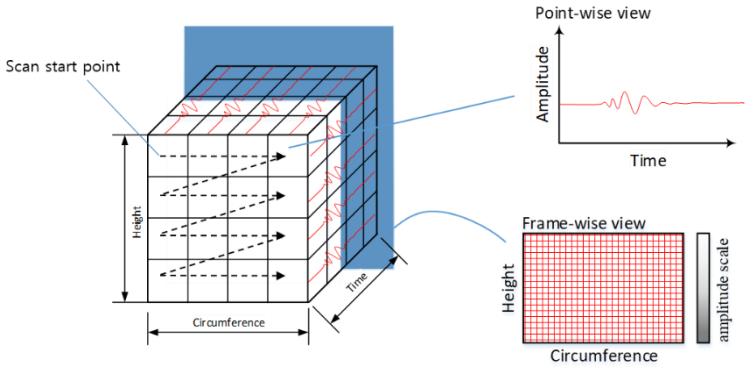

Fig. 5 Measurement storage and access

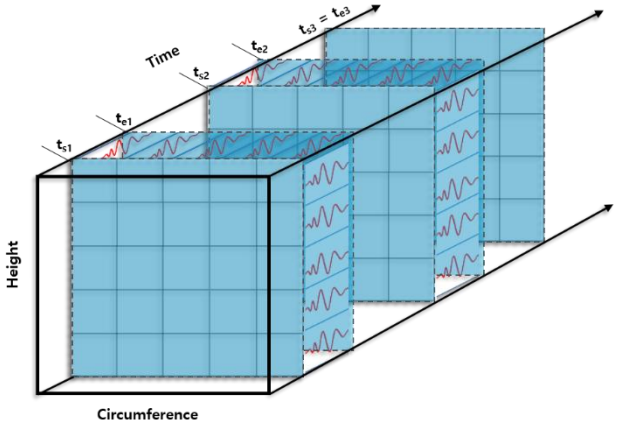

Fig. 6 mTWAM frame selection: An example of selecting three time windows for accumulation

inspection. This storage buffer is illustrated in Fig. 5, where the dotted line in the front shows the order in which the buffer was filled.

The measurement data can be accessed in a frame-wise manner by specifying a value for time (t), and the resulting frame is displayed as a two-dimensional intensity map. As explained in the previous section, the interval between consecutive measurements along the C or H dimension is denoted as I_L. This defines the spatial resolution of the inspection data as well as that of any frame. The individual frames when displayed along the T dimension show an ultrasonic wave propagation through the thickness of the specimen and can accurately display the subsurface features of the scanned specimen. This method of measurement visualization is called Ultrasonic Wave Propagation Imaging (UWPI) (Lee *et al.* 2018), which will be used to depict the inspection results in the next section. The measurement data can be accessed and viewed in a point-wise manner, whereby the $m(t)_{x,y}$ signal can be selected to be displayed as a one-dimensional signal.

2.4 Post-processing

A multi-Time Window Amplitude Map (mTWAM) (Lee *et al.* 2019) algorithm was implemented to effectively analyze the defects across multiple frames of the UWPI. Frames containing the defects or features of interest can be selected by the user after reviewing the UWPI freeze frames. The algorithm uses the selected frames from the memory buffer and combines them by performing an absolute summation across the frames for all the points in the frame.

The frames can be selected by selecting multiple time ranges of interest, and all the frames from the selected periods will be combined, as shown in Eq. (6).

$$\mathrm{V} = \sum_{i=1}^{n} \sum_{t=t_{si}}^{t_{ei}} |M(t)| \qquad \begin{cases} t_{si} < t_{ei}\,, & n = 1 \\ t_{si} \le t_{ei}\,, & n > 1 \end{cases} \tag{6}$$

where V is a two-dimensional structure of size ($C \times H$) that yields the results of the mTWAM algorithm; t_{si} and t_{ei} are the start and end of the i^{th} range selected, respectively; "n" specifies the total number of ranges selected at a time.

The minimum value for n is 1 when a single time range of interest is selected. In this case, both the start and end frames must be distinct to yield meaningful results. For cases when n is greater than 1, i.e., multiple ranges have been selected, the start and end of each time range may be the same or distinct, which results in the accumulation of separate frames or ranges of frames, respectively. Fig. 6 shows an example of frame selection, where three different ranges of interest are selected for accumulation. It is noteworthy the third range comprises only a single frame.

3. Results

To illustrate the performance of the R-PE_UPI system, the inspection results of the cylindrical specimens are presented herein. A band-pass filter developed in-house has been used for filtering the measurements in these inspections. It consists of an amplifier, a 24 dB/octave active Butterworth high-pass filter followed by an active Sallen-Key fourth-order low-pass filter (Thai *et al.* 2019).

3.1 Cylinder with wall thinning

The inspection results of a steel cylinder with wall-thinning defects are presented in this section. The steel cylinder has a diameter of 166 mm and a normal wall thickness of 8.8 mm. An oval-shaped wall-thinning defect was machined on the inside walls of the cylinder to

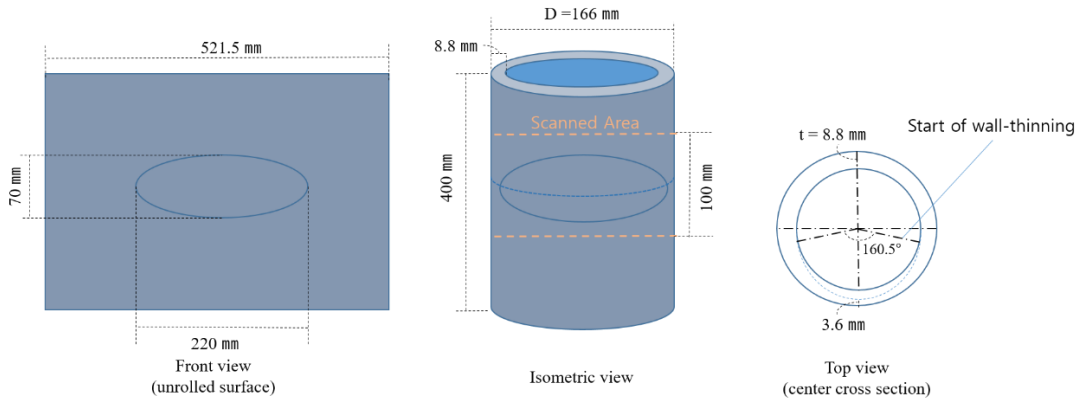

Fig. 7 Steel cylinder with oval-shaped wall thinning on the inside

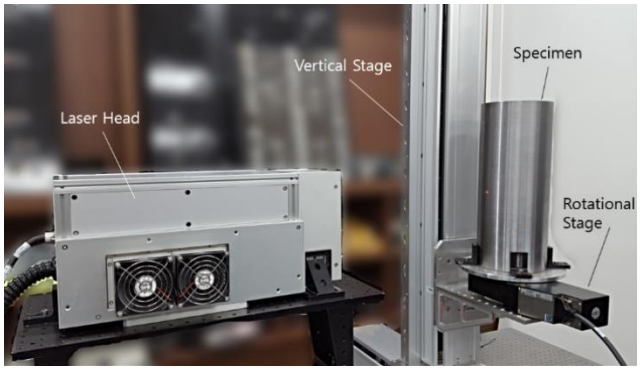

Fig. 8 Steel specimen inspection using R-PE_UPI system

highlight the subsurface damage detection capabilities of the R-PE_UPI system. In the wall-thinned area, the wall thickness of the cylinder decreased gradually from 8.8 mm, at the edges of the defect to 3.6 mm at its center. The defect is placed at the center along the length of the cylinder. Fig. 7 shows the specifications of the specimen and defect. The front view of the unrolled cylinder shows the placement and size of the defect. It is noteworthy that the results produced after scanning by the system were synonymous to this unrolled view, as the rotational scan line measurements were mapped to linear coordinates. The top view captured at the cross section along the major axis of the defect indicates a gradual change in wall thickness in the wall-thinned area.

The specimen was mounted on the rotational stage using a circular breadboard and brackets for inspection. Fig. 8 shows the system during the inspection of the specimen. Different components of the system are also shown in this image. The rotational stage was mounted on the vertical stage, which was part of the scanning system as explained in Section 2. The red laser point from the LDV was visible on the surface of the specimen. The specimen surface was cleaned prior to the inspection to achieve the optimum SNR of the measurements.

Table 1 summarizes the details of this inspection; a scan height of 100 mm and an appropriate scan start position were selected to incorporate all defects in the inspection. The range of the band pass filter was selected based on the material and wall thickness. An interval of 0.52 mm along with a maximum rotational scan speed of 80°/s was used for this inspection. This resulted in a scan time of 14.4 min, which was optimal owing to no braking or deceleration during the inspection while transitioning between the rotational scan lines. The LDV was placed at a stand-off distance of 438 mm from the inspected surface of the

Table 1 Steel cylinder inspection details

Specimen details	Material		Steel
	Thickness (mm)		Max: 8.8 Min: 3.6
	Diameter (mm)		166
	Defect		Oval shaped wall thinning inside the cylinder wall
Inspection settings	Scan settings	Scan height (mm)	100
		Interval I_L (mm)	0.52
		Rotational speed (°/s)	80
		Filter range (kHz)	500-750
	Excitation laser	Type	Q-switched pulsed laser
		Wavelength (nm)	1053
		Pulse energy (mJ)	3.5
		Pulse width (ns)	35
	Sensing laser	Type	LDV
		Wavelength (nm)	633
		Power (mW)	2
		Lens type	Medium range
		Stand-off distance (mm)	438

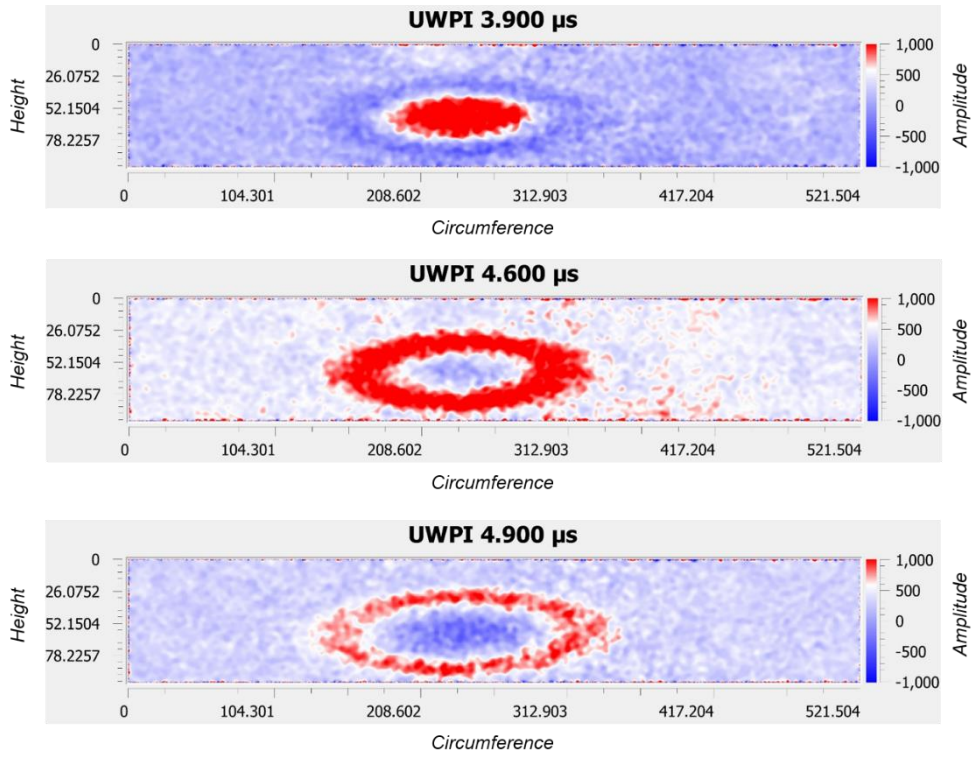

Fig. 9 Steel cylinder inspection results. UWPI freeze frames at 3.9, 4.6 and 4.9 µs showing wall thinning

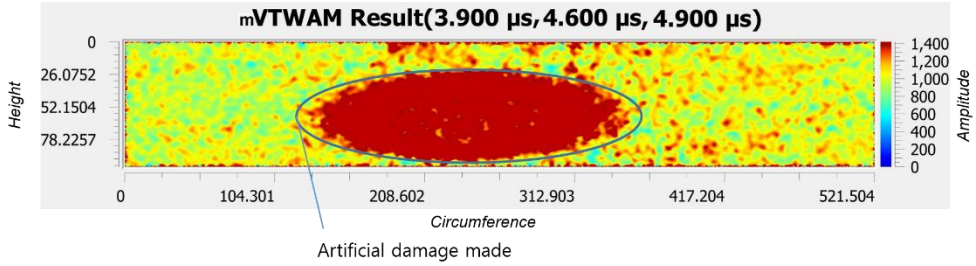

Fig. 10 mVTWAM result: Accumulation of UWPI freeze frame at 3.9, 4.6 and 4.9 µs showing the wall thinning oval shape with major axis length of 215 mm and minor axis length of 70 mm

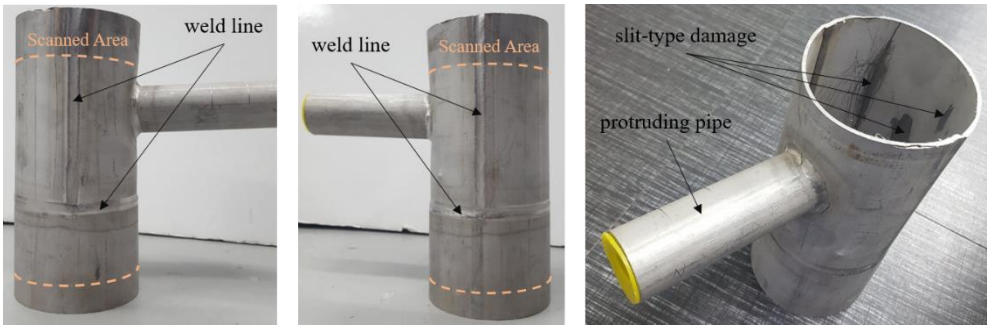

Fig. 11 Welded steel pipe specimen showing weld lines and slit-type damages

specimen and a medium range lens was used during this inspection.

The scan results were stored in memory and viewed in a frame-wise manner using the UWPI algorithm. The wall-thinning defect of the cylinder was visible in the UWPI frames. Fig. 9 shows the freeze frames of the UWPI at 3.9, 4.6, and 4.9 µs. It is noteworthy that owing to gradual change in wall thickness in the wall-thinning area, all the defects were covered in multiple frames of the UWPI. The mTWAM algorithm was used in post-processing to combine defect information from different frames. All the wall-thinned areas were visualized correctly in a single mTWAM

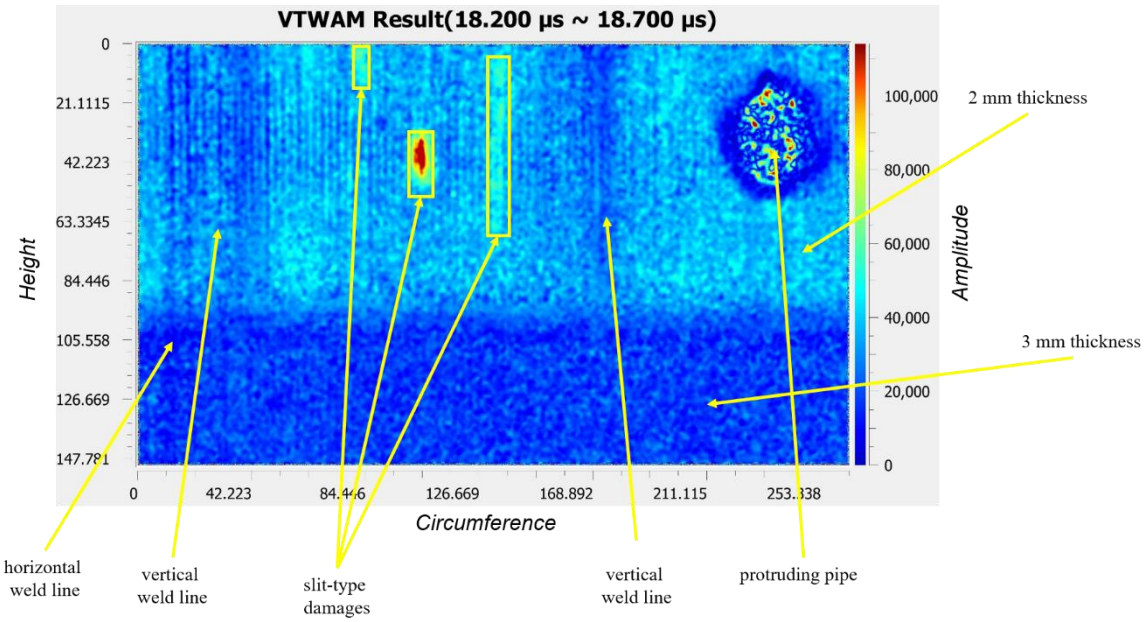

Fig. 12 Welded steel pipe VTWAM result; accumulation of UWPI freeze frame from 18.20-18.70 µs showing 3 slit damages of length 14 mm, 23 mm and 64 mm, from left to right, respectively. The weld lines and difference in wall thickness are also clearly visible

Table 2 Welded steel pipe inspection details

Specimen details	Material		Steel
	Thickness (mm)		2 (top part) 3 (bottom part)
	Diameter (mm)		85
	Defect		Silt-type damages made inside the steel pipe
Inspection settings	Scan settings	Scan height (mm)	150
		Interval I_L (mm)	0.21
		Rotational speed (°/s)	80
		Filter range (kHz)	50-250
	Excitation laser	Type	Q-switched pulsed laser
		Wavelength (nm)	1053
		Pulse energy (mJ)	2.3
		Pulse width (ns)	35
	Sensing laser	Type	LDV
		Wavelength (nm)	633
		Power (mW)	2
		Lens type	Medium range
		Stand-off distance (mm)	438

frame, as shown in Fig. 10.

3.2 Welded pipe

A pipe comprising radial pieces of steel welded together, was inspected using the system. As shown in Fig. 11, this steel pipe comprises three separate pieces, namely two radial pieces of thickness 2 mm each and a base pipe piece of thickness 3 mm. The two radial pieces were joined together with two vertical weld joints to form a pipe. This welded pipe was placed on the top of the base pipe piece and joined with another weld joint along the circumference of the pipe. Slit type damages appeared on the inside of the top pieces of the welded pipe, and a pipe of smaller radius was welded onto its surface.

This specimen was mounted on the rotational stage, which was then mounted on the vertical stage as part of the scanning system, as explained in Section 2. Table 2 summarizes the details of this inspection; a specimen height of 150 mm was scanned, and a scan start position was selected to include all the damages in the inspection. The total area scanned is shown in Fig. 11.

An interval of 0.21 mm along with the maximum rotational scan speed of 80°/s was used for this inspection. This resulted in a scan time of 53.3 min, which was optimal owing to no braking or deceleration during the inspection while transitioning between the rotational scan lines. A smaller interval was selected in this inspection to detect the long slit-type damage shown on the leftmost in Fig. 11. The LDV was placed at a stand-off distance of 438 mm from the inspected surface of the specimen and a medium range lens was used during this inspection.

Fig. 12 shows the VTWAM result, which was generated by accumulating UWPI frames from 18.20-18.70 µs. The two vertical weld lines and a circumference weld line were

visible in the results. The protruding pipe is shown as a circular feature in the inspection results. Finally, all the slit-type damages were visible. It is noteworthy that the bottom half of the inspection results are shown in distinct colors owing to the difference in thickness between the top and bottom plates.

4. Conclusions

The development and operation of a nondestructive inspection system for cylindrical specimens using laser-based excitation and sensing were presented herein. The system comprised of a 1053 nm solid-state Q-switched laser for generation and a 633 nm helium-neon LDV for the sensing of ultrasonic bulk waves traveling through the specimen wall. The LDV posed constraints on the position and orientation of the sensed specimen surface. First, the standoff distance between the LDV head and the inspected surface should remain constant throughout the inspection; next, the laser beam should be aligned to the normal of the surface during the inspection. These conditions were met for the cylindrical specimens based on a rotation scan for PE UPI. A rotational stage coupled with a single-axis linear stage was used in the system to scan the cylindrical specimen. This enabled the standoff distance and incidence angle constraints posed by the LDV sensor to be satisfied while obtaining the optimal SNR of the measured signals. Furthermore, the system supported the signal acquisition, processing, and result display in real time in parallel with the on-going inspection. The system blocks were synchronized to ensure no stoppage or scan speed reduction during the scan, thereby ensuring that the inspection was performed in a continuous scanning motion such that the minimum possible scan time was consumed for a predetermined scan resolution and stage speed. The capability of this system for cylindrical structural NDE was successfully proven with two real-world specimens.

Acknowledgments

This research was supported by the Ministry of Trade, Industry, and Energy (MOTIE), Korea, under reference number R0006462 supervised by the Korea Institute for Advancement of Technology (KIAT) and the National Research Foundation of Korea (NRF), grant funded by the Ministry of Science and ICT (NRF-2017R1A5A1015311).

References

Abbas, M. and Shafiee, M. (2018), "Structural health monitoring (SHM) and determination of surface defects in large metallic structures using ultrasonic guided waves", *Sensors*, **18**(11), 3958. https://doi.org/10.3390/s18113958.

Abbas, S.H. and Lee, J.R. (2018), "High-speed angular-scan pulse-echo ultrasonic propagation imager for in situ non-destructive evaluation", *Smart Struct. Syst., Int. J.*, **22**(2), 223-230. https://doi.org/10.12989/sss.2018.22.2.223.

Connolly, J.W. (2016), *In Understanding the Magic of the Bicycle*, Morgan and Claypool Publishers, San Rafael, USA. https://doi.org/10.1088/978-1-6817-4441-4ch10.

Flynn, E.B., Chong, S.Y., Jarmer, G.J. and Lee, J.R. (2013), "Structural imaging through local wavenumber estimation of guided waves", *NDT E Int.*, **59**, 1-10. https://doi.org/10.1016/j.ndteint.2013.04.003.

Hillger, W., Bühling, L., Ilse, D. and Büro, H.I. (2014), "Air-coupled ultrasonic testing-method, system and practical applications", *Proceedings of the 11th European Conference on Non-Destructive Testing (ECNDT 2014)*, Prague, Czech Republic, October.

Hong, S.C., Lee, J.R. and Park, J. (2016), "Composite NDE using full-field pulse-echo ultrasonic propagation imaging system", *Proceedings of the Active and Passive Smart Structures and Integrated Systems*, Nevada, USA, March.

Lee, C. and Park, S. (2015), "Damage visualization of pipeline structures using laser-induced ultrasonic waves", *Struct. Health Monit.*, **14**(5), 475-488. https://doi.org/10.1177/1475921715596220.

Lee, J.R., Chong, S.Y., Jeong, H. and Kong, C.W. (2011), "A time-of-flight mapping method for laser ultrasound guided in a pipe and its application to wall thinning visualization", *NDT E Int.*, **44**(8), 680-691. https://doi.org/10.1016/j.ndteint.2011.07.005.

Lee, Y.J., Lee, J.R. and Ihn, J.B. (2018), "Composite repair patch evaluation using pulse-echo laser ultrasonic correlation mapping method", *Compos. Struct.*, **204**, 395-401. https://doi.org/10.1016/j.compstruct.2018.07.124.

Lee, W.J., Seo, B.H., Hong, S.C., Won, M.S. and Lee, J.R. (2019), "Real world application of angular scan pulse-echo ultrasonic propagation imager for damage tolerance evaluation of full-scale composite fuselage", *Struct. Health Monit.*, **18**(5-6), 1943-1952. https://doi.org/10.1177/1475921719831370.

Panwar, R. and Lee, J.R. (2018), "Performance and non-destructive evaluation methods of airborne radome and stealth structures", *Meas. Sci. Technol.*, **29**(6), 062001. https://doi.org/10.1088/1361-6501/aaa8aa.

Petcher, P.A. and Dixon, S. (2017), "Mode mixing in shear horizontal ultrasonic guided waves", *Nondestruct. Test. Evaluation*, **32**(2), 113-132. https://doi.org/10.1080/10589759.2016.1184268.

Rose, J. (2014), *Ultrasonic Guided Waves in Solid Media*, Cambridge U Press, New York, USA.

Schmerr Jr, L.W. (2016), *Fundamentals of Ultrasonic Nondestructive Evaluation*, Springer, Switzerland.

Schrapp, M., Scharrer, T., Goldammer, M., Rupitsch, S.J., Sutor, A., Ermert, H. and Lerch, R. (2013), "Artifact reduction in non-destructive testing by means of complementary data fusion of x-ray computed tomography and ultrasonic pulse-echo testing", *Meas. Sci. Technol.*, **24**(12), 125403. https://doi.org/10.1088/0957-0233/24/12/125403.

Scruby, C.B. and Drain, L.E. (1990), *Laser Ultrasonics-Techniques and Applications*, CRC Press, New York, USA.

Sohn, Y. and Krishnaswamy, S. (2004), "Interaction of a scanning laser-generated ultrasonic line source with a surface breaking flaw", *J. Acous. Soc. Am.*, **115**(1), 172-181. https://doi.org/10.1121/1.1630997.

Thai, M.T., Ahmed, H., Hong, S.C., Lee, J.R. and Ihn, J.B. (2019), "Broadband laser ultrasonic excitation and multi-band sensing for hierarchical automatic damage visualization", *Int. J. Aeronaut. Space Sci.*, **20**(4), 913-932. https://doi.org/10.1007/s42405-019-00210-4.

White, R.M. (1963), "Generation of elastic waves by transient surface heating", *J. Appl. Phys.*, **34**, 3559-3567. https://doi.org/10.1063/1.1729258.

Zhang, H., Xu, C. and Xiao, D. (2018), "Crack assessment of wheel hubs via an ultrasonic transducer and industrial robot", *Sens. Transducers*, **18**(12), 4336.

https://doi.org/10.3390/s18124336.
Zhang, K., Li, S. and Zhou, Z. (2019), "Detection of disbonds in multi-layer bonded structures using the laser ultrasonic pulse-echo mode", *Ultrasonics*, **94**, 411-418. https://doi.org/10.1016/j.ultras.2018.06.005.

HJ